



Research Paper

Fission gas released from molten salt reactor fuel: the case of noble gas short life radioisotopes for radiopharmaceutical application

Claude Degueldre^{a,*}, Richard Dawson^a, Isabel Cooley^b, Elena Besley^b^a Engineering Department, Lancaster University, LA1 4YW, UK^b School of Chemistry, University Park Nottingham, NG7 2RD, UK

ARTICLE INFO

Keywords:

Molten salt reactor
Noble gas radioisotopes
Radio-diagnostics
Radiotherapy

ABSTRACT

The present study explores the potential of fission gas (Kr and Xe short life radioisotopes) released from a molten salt reactor, the separation of these noble gases using specific absorbents under well fixed conditions and the utilisation of these radioisotopes for radio-diagnostics. During operation, a molten salt reactor produces noble gas radioisotopes that bubble out from the liquid fuel and that can be sampled and treated for radiopharmaceutical applications including as tools for diagnostics using γ radioisotopes and/or potentially in radiotherapy for specific viral diseases using β^- emitters. Among them ^{133}Xe is currently used for lung diagnostics thanks to its 132.9 keV γ . The use of ^{85}Kr for diagnostics is also examined. Its 514 keV γ could be used for scintigraphy. However ^{133}Xe utilisation imply also its β^- ($E_{\text{mean}} \approx 100$ keV) whose mean free pathway of 100 nm in biological tissue or in water is much smaller than the mean pathway of the ^{95}Kr β^- . Emphasis is placed on ^{133}Xe because of its potential dual ability of imaging and as a suggested therapeutic tool of viral lung diseases.

1. Introduction

In the last decades, the development and production of pharmaceutical agents using radionuclides has been a growing field for molecular imaging, radiotherapy and medical research as reported by Crestoni (2018) [1] in the last review paper dealing with radio-diagnostics and radiotherapy. This interdisciplinary approach exploits fast and non-invasive modalities for:

- (i) Radio-diagnostic imaging of several diseases and real-time clinical monitoring via single-photon emission computed tomography and positron emission tomography;
- (ii) radiotherapy via emission of particulate, ionizing radiation, alpha (α) and beta (β^-) particles, and Auger electrons, depositing energy in tissues and causing cell death or virus resorption.

Several nuclides for imaging (^{11}C , ^{18}F , $^{99\text{m}}\text{Tc}$, ^{64}Cu , ^{68}Ga , ^{89}Zr , ^{111}In) and therapy (^{90}Y , ^{131}I , ^{153}Sm , ^{188}Re , ^{223}Ra , ^{225}Ac) have been successfully incorporated into radiopharmaceuticals approved protocols or are under ongoing clinical trials as noted by Crestoni (2018).

Now, it must be noted that Xe and Kr isotopes are absent from Crestoni's review, which may be because these isotopes are less used

than the above mentioned one and their inertness does not allow association onto specific molecules that are typically used in radio-pharmacy. They should be revisited for diagnostics and investigated for radio-therapy. Xenon-133, with its 5.25 days half-life, is nowadays known to be used for lung diagnostics (γ -radioscopy/tomography) such as reported by Parker et al. (2012) [2]. This methodology was developed some 50 years ago, see Lull et al. (1983) [3] and Graban (1969) [4]. Bailey and Roach (2020) [5] reported a brief history of lung imaging over the last 50-years in nuclear medicine quoting the flexibility of xenon-133.

Radioactive isotopes of xenon and krypton are being released from molten salt reactor during operation as volatile fission products and in principle could be part of the radioactive waste material. These isotopes should not be considered as nuclear waste materials since they are acknowledged for their application as diagnostic based reagents in nuclear medicine. Among them ^{133}Xe is well known for its use as a γ tracer for the diagnostic of lung diseases.

The present paper revisits the use of xenon and krypton radioisotopes for radio-diagnostics but also for β^- radiotherapy of viral lung diseases.

2. Noble gas radioisotope production from MSR

Molten Salt Reactors (MSRs) are liquid fuel reactors where, in its

* Corresponding author.

E-mail address: c.degueldre@lancaster.ac.uk (C. Degueldre).

classical design, the fuel is also the coolant. They have been the fruit of intensive R&D projects in the 50's, 60's and 70's at the Oak Ridge National Laboratory e.g. Weinberg (1979) [6] which built the basis of the science of the molten salt reactors. These reactors are safer than the standard light water reactors (LWR) as reported by MSR safety experts e.g. Elsheikh (2013) [7] and run with larger EROEI factor (around 1000) than the commercial LWR (110-11) Huke et al. (2015) [8]. The implantation of molten salt reactors for example as Small Modular Reactors (SMRs) has been suggested by Zou et al. (2020) [9], and by Kang et al. (2020) [10], together with optimisation of neutron economy and fissile management in a specific nuclear fuel cycle as proposed by Degueldre et al. (2019) [11]. The design of the SM-MS Reactor (see Fig. 1) deals with key challenges such as the optimisation the reactor for flexible use and production. With the solubility increase of xenon in alkaline/earth alkaline/actinide molten salt phase during temperature increase, the neutron economy is degraded by the build-up of strong neutron absorbers such as ^{135}Xe .

During MSR operation, fission products generated in the core of the reactor subsequently flow in the primary loop. Some of them are strong poisons absorbing neutrons and are unsuitable isotopes. Among them ^{135}Xe (half-life 9.1 h) has the largest neutron capture cross section (2.6 million barns) of all the known isotopes. Its father nuclide ^{135}I with its half-life of 6.61 h contributes to ^{135}Xe concentration build-up. Similarly, the isotope ^{83}Kr has a neutron capture cross section of 183 b and its elimination is also desirable. The behaviour and properties of Kr, Xe and their precursor I in fluoride and chloride molten salts have been addressed by Smirnov et al. (1988) [12]. Actually, isotopes of Xe and Kr acting as neutron poisons are generally countered by a high fuel loading which may be a source of economic issues. For iodine the case is evident, ^{135}I decays into ^{135}Xe that can affect reactor reactivity and reduce the energy production e.g. Eades et al. (2016) [13].

There are several strategies to eliminate the excess of ^{135}Xe such as its decay process, its degassing or its ventilation. The evolution of ^{135}I and ^{135}Xe which are entrained in the flowing salt, may be evaluated for its concentration change with the burn-up time Ref. Wu et al. (2017) [14]. A

fast circulation of fuel salt could decrease the concentration of ^{135}I and ^{135}Xe , and the reduction can achieve purging of around 50 and 40% for ^{135}I and ^{135}Xe respectively at a small power level, e.g. 2 MW, when the core has the same fuel salt volume as that of the outer-loop. Similarly ^{133}I decays in ^{133}Xe which is of interest in this study it can after collection of the xenon isotopes be separated from ^{135}Xe by decay (see isotope half lives in Table 1). The second possibility is to use helium (less soluble) to remove the more soluble Xe.

The release of fission product and salt compounds from a molten salt reactor fuel under elevated temperature conditions has been investigated by Kalilainen et al. (2020) [15] with coupled computer simulations. The thermodynamic modelling of the salt and fission product mixture was performed using the Gibbs Energy Minimization Software GEMS. The

Table 1

Nuclear properties of noble gas isotopes released from MSR as given by Pfenning et al. (1998) [18] and Holden (2004) [19].

Isotope	Decay	β energy MeV	X-ray & γ energy keV	Half life	Daughter isotope 1
^{125}Xe	β^-	0.3	55, 188, 243	16.9 h	^{125}I
^{133}Xe	β^-	0.3	31, 81	5.2475 d	^{133}Cs
^{133m}Xe	γ	e^- Auger	233	2.19 d	^{133}Xe
^{135}Xe	β^-	0.9	250, 608	9.14 h	^{135}Cs
^{79}Kr	β^-	0.6	261, 398	35.04 h	^{79}Br
^{85}Kr	β^-	0.7	514	10.776 y	^{85}Rb
^{85m}Kr	β^-	0.8	151, 305	4.480 h	^{85}Rb
^{88}Kr	β^-	0.5, 2.9	2392, 196	2.84 h	^{88}Rb

Daughter isotope 1	Decay	β energy MeV	X-ray & γ energy keV	Half life	Daughter isotope 2
^{125}I	β^-	0.2	35	59.4 d	^{125}Te
^{135}Cs	β^-	0.2	No	2×10^5 a	^{135}Ba
^{79m}Br	γ	0.6	207	3.9 s	^{79}Br
^{88}Rb	β^-	5.3	1836, 898	17.8 m	^{88}Sr

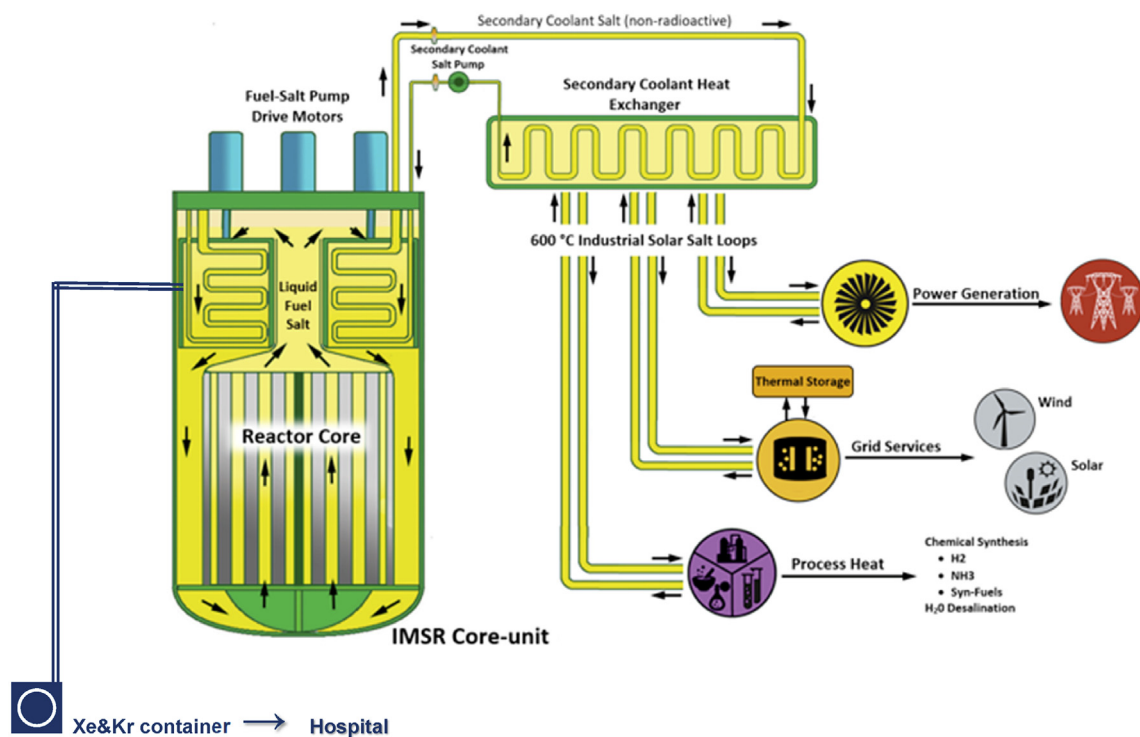


Fig. 1. Small modular molten salt reactor with its energy production (right) and its isotope production line for Xe & Kr (left). IMSR picture, adapted for the isotope extraction line on the left and bottom, original plant cross section from Terrestrial Energy as reported by LeBlanc (2018) [17].

fuel salt considered in the simulations was LiF-ThF₄-UF₄ with fission products Cs and I. The results were compared to simulations using pure compound vapour pressures in the evaporation simulations. It was observed that by modelling the salt mixing, the release of fission products and salt materials was reduced when compared to the pure compound simulations. The mixing effects in the salt, when compared to the pure compound simulation also affected evaporation temperatures and therefore the timing of the release of compounds. The analysis of the fission product volatilisation and sorption is carried out by mass spectroscopy which is more sensitive than that reported earlier e.g. Akerib et al. (2018) [16]. Surprisingly, experimental data show that xenon is more soluble at high temperature than just above the melting point. Xenon purging is consequently recommended after the heat exchanger. Fig. 1 presents a schematic picture of the SM-MSR including the module for the treatment of fission products (FP absorber) and from where the collection of Xe and Kr is carried out.

The potential of the production of specific fission gas radioisotopes for medical applications ¹²⁹Xe and ¹³³Xe used for lung (and brain) imaging must be explored.

3. Nuclear properties of xenon and krypton radioisotopes

For practical reasons, interest is set on isotopes with half-life larger than 1 h (see Table 1). Decay's nuclides include both β^+ and β^- emitters while isotopes produced as fission products are generally heavier radioisotopes (than the natural isotopes) which are usually β^- emitters. Daughter products are added as they are potentially also radioactive nuclides. These nuclear properties of noble gas isotopes released from MSR guide us for their selection as radio-diagnostic and radio-therapy tools.

Among them, one krypton and one xenon radioisotopes ⁷⁹Kr (β^+) and ¹²⁵Xe (β^+) respectively could be used as PET isotopes. However, the fission yield for the production of light isotopes is rather low compared to heavy, restricting their production.

Three krypton radioisotopes ⁸⁵Kr(β^-), ^{85m}Kr(β^- - γ) and ⁸⁸Kr(β^-) are found with $E_\beta < 0.5$ MeV.

Three xenon radioisotopes ¹³³Xe(β^- - γ), ^{133m}Xe(γ) and ¹³⁵Xe(β^- - γ), the later with $E_\beta < 0.5$ MeV.

To complete the view, decay products are also considered in Table 1.

The selection of 133-xenon may be justified as follows.

The mean free pathways of the β^- particles as a function of their energy was recently estimated by Incerti et al. (2018) [20]. Calculations were carried out using Geant4DNA applied for track structure simulations in liquid water as analogue of soft tissues, see Fig. 2. Since biological systems (cells, bacterias, viruses) are made of light structural biomaterial with a rather large proportion of water, the mean free pathway in water can be used in a first approximation. Since it is a key parameter to estimate the distance between successive impacts (interactions), it is a key parameter to select the energy of the β emitter in radiotherapy.

Clearly, the pathway was found to decrease when increasing the interactions.

The following statements guide our strategy:

1. Since the average energy of ¹³³Xe (5.2475 d) β is 100 keV (with a maximum of 300 keV), its mean free pathway in biomaterial (virus) is about 100 nm E_{mean} and 300 nm for E_{Max}
2. The size of corona virus is 80 nm (125 nm with the spikes) its penetration fits with the object size and one may anticipate it could be used for therapy ... In addition the ionization effect is strong at the path-length end ...
3. However ⁸⁵Kr (10.76 years) decays with β energy of 700 keV with could be too high in energy for the corona virus treatment (mean free pathway in biomaterial (virus) is about 300 nm, co-irradiation of lung

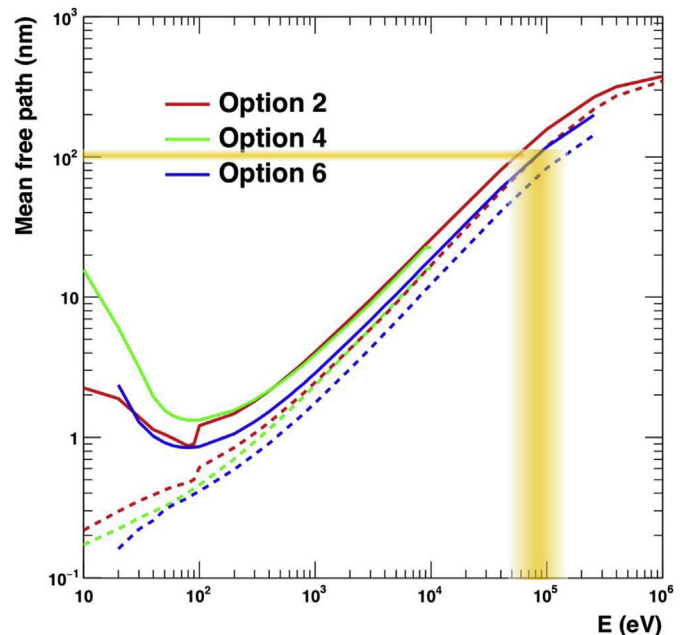


Fig. 2. Mean free pathway of the electron or the beta particle as a function of their energy, calculated for water as a function of incident particle energy. Simulations using the three Geant4 standard EM physics models, modified for medium density, followed three options corresponding to increasing interactions:

- Option 2 (default model) was a first set of discrete physics models implemented in Geant4 for electron transport in liquid water down to eV energies.
- Option 4 offered alternative discrete physics models to “option 2” for electron transport in liquid water in the 10 eV–10 keV energy range with updated cross sections for electron-impact excitation and ionization in liquid water, and an alternative elastic scattering model.
- Option 6 was another alternative set of discrete physics models for electron transport in liquid water over the 11 eV–256 keV energy range with implementation of specific interaction cross sections.

tissues) in addition its half-life is 10 days, meaning it maintains a certain activity in the body after treatment (even if its biological half live is much smaller). A ¹³³Xe treatment is consequently recommended ...

Conditions: dashed lines: for all physical interactions, solid lines: for inelastic interactions only; the “mean free path” is simulated using the three Geant4 standard EM physics models, modified for medium density, see Incerti et al. (2018), following Options 2, 4 & 6 (increasing interactions):

- Option 2 (default model) is the first set of discrete physics models implemented in Geant4 for electron transport in liquid water down to eV energies.
- Option 4 offers alternative discrete physics models to “option 2” for electron transport in liquid water in the 10 eV–10 keV energy range with updated cross sections for electron-impact excitation and ionization in liquid water, and an alternative elastic scattering model.
- Option 6 is another alternative set of discrete physics models for electron transport in liquid water over the 11 eV–256 keV energy range with implementation of specific interaction cross sections.

Since both noble gas radioisotopes have different nuclear properties, their separation is mandatory when one has to utilise ¹³³Xe because of its smaller mean energy and shorter half-life compared to ⁸⁵Kr.

4. Krypton/xenon separation

Effective separation of Xe and Kr has been traditionally achieved by the slow and costly method of cryogenic distillation, e.g. Banerjee et al. (2018) [21]. More efficient alternative approaches such as pressure swing and temperature swing adsorption (PSA and TSA), and membrane-based separations are based on physical sorption where specific porous adsorbents are used to preferentially adsorb either Xe over Kr or the reverse. Porous material, including activated carbon, e.g. Thallapally et al. (2012) [22], zeolites, as in Jameson et al. (1997) [23], organic cages, Chen et al. (2014) [24] and more recently metal-organic frameworks (MOFs) Chung et al. (2019) [25] have been assessed for their selectivity and adsorption capacity. Whilst experimental measurements of Xe/Kr separations are carried out for individual materials, rapid computational screening of databases for useful properties, as shown by Sikora et al. (2012) [26], Ryan et al. (2011) [27], as well as *in silico* design of hypothetical structures, e.g. Wilmer et al. (2011) [28], can be invaluable in guiding experimental efforts.

Assisting experimental efforts, several computational screenings have indicated promising porous structures for Xe/Kr separations and have examined structure-function relationships, revealing that optimal pore sizes have a significant impact on selectivity. Pores close to the size of a Xe atom exhibit an effect in which a Xe atom experiences strong interactions on all sides with a narrow-pored framework, see Sikora et al. (2012) [27] and Simon et al. (2015) [29]. Screenings have also shown that cylindrical pores are more likely to display higher selectivity than spherical pores, although successful binding site geometry can vary, e.g. Sikora et al. (2012), Simon et al. (2012).

Computational screenings and experimental studies of Xe/Kr separation typically use either a 1/4 Xe/Kr mixture at room temperature and pressures close to 1 bar, e.g. Sikora et al. (2012), Simon et al. (2012), or so-called nuclear reprocessing conditions (10 Xe/Kr at room temperature), see Liu et al. (2012) [30], Banerjee et al. (2016) [31]. These sets of conditions are intended to replicate the common sources of a Xe/Kr mixture: the first as a product of cryogenic distillation of air and the second as a product of nuclear reprocessing for which the aim is removal and storage of radioactive isotopes. However, these conditions do not reflect requirements for separation for further use of Xe and Kr isotopes as products of an MSR, particularly in terms of the high temperature of MSR products (600–800 °C). The latter requirements, along with the time-sensitive nature of the separation, are generally not explicitly considered.

In physical-sorption-based separation studies, there has been limited consideration of adsorption at very high temperatures or at cryogenic temperatures. To consider the performance of a material at elevated temperature, a number of factors must be examined. First, it must be established whether the structure is thermally stable at the desired temperature, and subsequently altered adsorption and diffusion behaviour due to the change in temperature must be assessed. Altered behaviour may be either due to altered energetics and dynamics of guests or to newly introduced flexibility of the framework.

In terms of thermal stability, activated carbons would be a promising option. However, they are considered unsuitable for nuclear reprocessing because of the associated hazard of bed fires, as discussed in Banerjee et al. (2018), and in any case their selectivity performance is often far inferior to the more advanced counterparts, see Thallapally et al. (2012). Certain zeolites are able to possess very high thermal stabilities, with temperature of structural collapse ranging from around 200 °C to more than 1000 °C, Cruciani et al. (2006) [32]. Stable structures at working temperatures therefore exist and may be promising.

Benchmark MOFs possess greater tunability and exhibit higher selectivity and capacity than the best-performing zeolites at more commonly studied temperatures, e.g. Banerjee et al. (2018), Although those with stability up to 600–800 °C have not yet been identified. Zeolitic imidazolate frameworks are examples of MOFs which are isostructural with zeolites. They possess relatively high thermal stabilities

up to 550 °C, see Park et al. (2006) [33]. MOFs with small pore sizes also display relatively high thermal stability Banerjee et al. (2018). This is fortunate for this study as pores on the order of the diameter of Xe are already established as optimum for selectivity under previously studied conditions, e.g. Sikora et al. (2012) and Simon et al. (2015). Indeed, a promising Xe/Kr selective MOF, **SBMOF-1**, synthesized by Cruciani et al. (2006), possesses a relatively high thermal stability of up to 230 °C. It is possible that a MOF with similar structure and performance, if any, may be useable under working conditions.

A structure's stability at high temperature and strong performance at room temperature do not guarantee its strong performance over all temperatures. As an example of temperature dependent adsorption properties, a partially fluorinated MOF(Cu), **FMOFCu**, was found by Fernandez et al. (2012) [34] to reverse its Xe/Kr selectivity on temperature change, with higher uptake of Xe than Kr above room temperature, and the reverse at lower temperatures. Such an extreme change is not common, e.g. Banerjee et al. (2018), but it is reasonable to expect that temperature effects may be observed under MSR conditions. It must be considered that in adsorption studies in general, total loading is expected to decrease as temperature increases (this being the principle behind TSA processes, see Ben-Mansour & Qasem (2018) [35], meaning efficiency of the separation may be compromised. Assuming this decrease in capacity, an appropriate adsorbent for use at MSR conditions would require an exceptional performance at room temperature.

The separation method is also significant. For membrane separations, not only gas loading but also permeability is important, and this measure has been shown to increase with temperature, see Huang et al. (2010) [36], potentially also leading to increase in selectivity. This has been examined for the case of Xe/Kr separations. A computational study of Hasanzadeh et al. (2020) [37] assessed the temperature dependence of Xe/Kr separation by the chabazite (CHA) zeolite membrane. It is suggested that membrane separation is possible, and permeance improved with temperature, up to at least 430 °C. The structure has pore diameters below that of a Xe atom, meaning the simulation was largely not complicated by competitive Xe adsorption or permeance. This is an example of the significance of geometry-based effects at a temperature where specific interactions may contribute less to selectivity. This, or a similar structure, could be promising for the required applications, although the simulation used here was on a small scale. Further work is needed to establish the efficacy of CHA or similar zeolites and whether scale-up is feasible for industrial application. It could also establish whether any promising MOF structures may exist, and further examine the general viability of physisorption-based methods at high temperatures.

When attempting assessment of high temperature adsorption processes, the increased effect of framework flexibility may become an issue. There are cases, even at room temperature, in which structural flexibility is shown to be the explanation for observed adsorption properties, see Schneemann et al. (2014) [38] and Yang et al. (2011) [39]. Flexibility becomes more pronounced as temperature increases, Fernandez et al. (2012): the selectivity reversal in **FMOFCu** is thought to be the result of framework flexibility above room temperature and rigidity below, e.g. Chen et al. (2013) [40]. This is likely to be significant under MSR conditions and will present a particular issue for computational studies. Specific, although costly, models may be developed for individual systems and are necessary at high temperature limiting the potential of large-scale studies, as shown by Yang et al. (2011) and Chen et al. (2013).

Similar to high temperatures processes, altered behaviour may be displayed at cryogenic temperatures when compared to ambient conditions. An advantage of cryogenics is that structural flexibility is unlikely to be significant. However, modelling at low temperatures presents its own challenges for structures containing open metal sites, Chen et al. (2011) [41]. It is common for simulations to underpredict interactions with the open metal site, and this effect is pronounced when temperature is low. To our knowledge there have been no studies of an adsorption-based Xe/Kr system at cryogenic temperatures, so further

work would be required to establish separation properties under these conditions.

For the application of MSR product radioisotopes, it is necessary to consider the timescale of a separation. For the isotopes considered, with half-lives on the scale of days, it is important that any separations whose products are intended for use are rapid. This can be established through use of breakthrough studies. Experimentally, such breakthrough studies at and close to room temperature exist for Xe/Kr systems, e.g. Liu et al. (2012) and Banerjee et al. (2016), and they show that the separation can be achieved on the scale of minutes to just over an hour. Naturally, separation times depend on the system and must be individually assessed for a given setup. With the temperature dependence of gas permeability, timescale could be a significant issue if using cryogenic conditions but would be unlikely to pose a problem at high temperatures, see Huang et al. (2010) and Hasanzadeh et al. (2020). In computational studies, simulated breakthrough curves are not common but have been generated, for example by Qasem et al. (2018) [42]. Molecular dynamics calculations of diffusivity may also give an indication of the time-dependence of a separation, e.g. Daglar et al. (2018) [43] and Adatoz et al. (2015) [44].

Finally, when selecting a MOF material for a separation application, the potential for residual synthesis solvent to affect adsorption processes must be assessed. During synthesis it is standard to remove solvent by an activation process. If solvent removal is incomplete it has been shown by Vitrillo et al. (2017) [45] and Konik et al. (2019) [46] that in certain cases the presence of residual solvent in pores can have a notable effect on the adsorption properties of a given MOF, influencing interaction strength and selectivity. Since computational studies generally assume an ideal sample, they will not as a rule include solvent effects. A high-throughput screening considering the effects of bound solvent on the Xe/Kr separation has been carried out by Chung et al. (2019) and it was found that Xe adsorption could become both more and less favourable when bound solvent is removed, as solvent can either block or form part of a favourable adsorption site. This study was at room temperature, so for applications at high or cryogenic temperatures further consideration of solvent effects would be needed. It could be supposed that under MSR conditions temperatures would be high enough that any solvent would no longer be bound. This is supported by TGA experiments in which mass loss for solvent finishes at lower temperatures than the MSR conditions, see Park et al. (2006) and Fernandez et al. (2012). However, as shown by Park et al. (2006), there exist structures for which mass loss for solvent is not sharp and continues to relatively high temperatures. Additionally, if other gases were present in the stream, they may compete for adsorption in a similar manner to solvent molecules, even if the framework was initially evacuated. Although at high temperatures solvent effects are unlikely to be a pressing issue, considering their presence may prove useful.

5. Application and discussion

5.1. Application

The fission gas mix released from nuclear fuel has a Kr/Xe ratio of the order of 1/8 (molar ratio). A Kr–Xe separation is recommended to avoid cumulative effect of both emitters. Practical separation (pragmatic/fast) has to be adapted using specific adsorbents, see also Liu et al. (2012) and Banerjee et al. (2016). Experimental expertise is required to find the easiest separation using a robust adsorbent (e.g. a zeolite). Radio-xenon isotopes can then be stored carefully prior to medical application and during time $^{133\text{m}}\text{Xe}$ and ^{135}Xe activities decreases.

At the time of calibration, the prepared gas contained no more than 0.3% xenon-133 m; not more than 1.5% xenon-131 m; **not more than 0.06%** krypton 85 and not more than 0.01% iodine 131 with not less than 99.9% of the radioactivity originating from the radioxenon known to behave in the body as non-radioactive xenon. This composition will change over time (cf. radioactive decay then possible leaks, after pouring

into the experimental container). For example, the ^{133}Xe “multi-injection” bottles used in the 1960s and early 1970s lost 5–6% of their xenon per day (even when stored closed). This type of leakage can be reduced by 70–80% by cold. Similarly, a plastic syringe containing a xenon solution spontaneously loses ½ to 1% of its content per hour. It has also been shown that xenon, which is relatively sparingly soluble in saline solutions, could be released from a solution and percolate into the rubber seal of the plunger of this syringe. A 2.5 cm³ syringe containing 0.5 ml of a xenon solution can lose up to 50% of its xenon in 2 h for an activity of 100 MBq, about 20–50 MBq can be deposited (or sorbed) in the tubing, valve and vessel. Therefore quantification in-vivo must definitively be carried out prior and diagnostic and treatment.

An accurate control of the ^{133}Xe and radio-traces of other radio-xenon and radio-krypton isotopes need to be assessed prior performing full **radio-diagnostic** investigation and carrying out the radio-therapeutic processes. Radio-xenon γ spectra are first recorded to quantify for estimating concentrations (using gamma data) and for evaluating in situ doses (using beta data) as proposed by McIntyre et al. (2016) [48]. This combination allows full quantification of the doses of the xenon radioisotope in-situ (e.g. in the lung). Fig. 3a presents the experimental spectra plotted for ^{133}Xe (γ) and minor amount of ^{135}Xe . The gamma spectrum recorded in this case for large scintillation crystal, i.e. NaI(Tl) with 8.9 cm outer diameter and 11.1 cm long (McIntyre et al. (2016), the ^{133}Xe activity deposited in the lung alveoli is estimated from the **gamma** peak at 80 keV gives for a fixed activity a given counting rate. Once assessment of radio-xenon's is carried out, radiography and tomography may be carried out to image the distribution of the fat nodules and the concentration of lipid phases due to viral aggregates. Note that the absorption coefficient taken for soft tissues (as water) is $\mu = 0.1837 \text{ cm}^{-1}$ and for 5–10 cm sub-thoracic organ a correction due to an absorption of about 60–90% has to be applied.

The in-situ beta doses can be deduced and can be adapted by inhalation time adjustment. The beta-simulations that incorporated GEANT-modeled data sets from ^{133}Xe decay, as well as functionality to use detector-acquired data sets to create new beta-spectra with varying amounts of background, ^{133}Xe and its decay products are given in Fig. 3b. During the radiotherapy treatment, the ^{133}Xe beta activity estimated for 100 keV (e.g. 75–150 keV) is maintained below the radiological threshold. (Exposure to radiation during a medical procedure needs to be justified by weighing up the benefits against the detriments that may be caused.)

Note:

- during the **radio-diagnostic** phase, the ^{133}Xe activity deposited in the lung alveoli is estimated from the **gamma** peak at 80 keV (Plum) recorded with a NaI(Tl). Radio-traces of ^{135}Xe are also detected at 250 keV (Orange).
- during the treatment (**radiotherapy**), the ^{133}Xe **beta** activity estimated for 100 keV (Dark yellow) is maintained below the radiological threshold

5.2. Discussion

In the human body, ^{133}Xe is a readily diffusible gas, which passes through cell membranes and freely exchanges between blood and tissue. It tends to concentrate more in pulmonary **fat nodules**, as shown by Yeh & Peterson (1963) [49], than in blood, plasma, water or protein solutions, e.g. Weathersby & Homer (1981) [50]. Solubility of Xe in water at 20 °C is 0.6 g L⁻¹ which is rather poor (Fig. 4). It is however the largest solubility of noble gases in water (excepting Rn).

From Fig. 4 the solubility of xenon at 30 °C in water is found to be 0.47 mg Xe per mL solvent (water). Data have been tabulated from more than 150 references on the solubility of inert gases in fluids and tissues of biological interest, Ref. Weathersby & Homer, (1981). Thirty-two gases have been studied in blood with measured solubility ranging from 0.005 to 16 ml of gas at 37 °C per ml of blood. For most gases, solubility in other

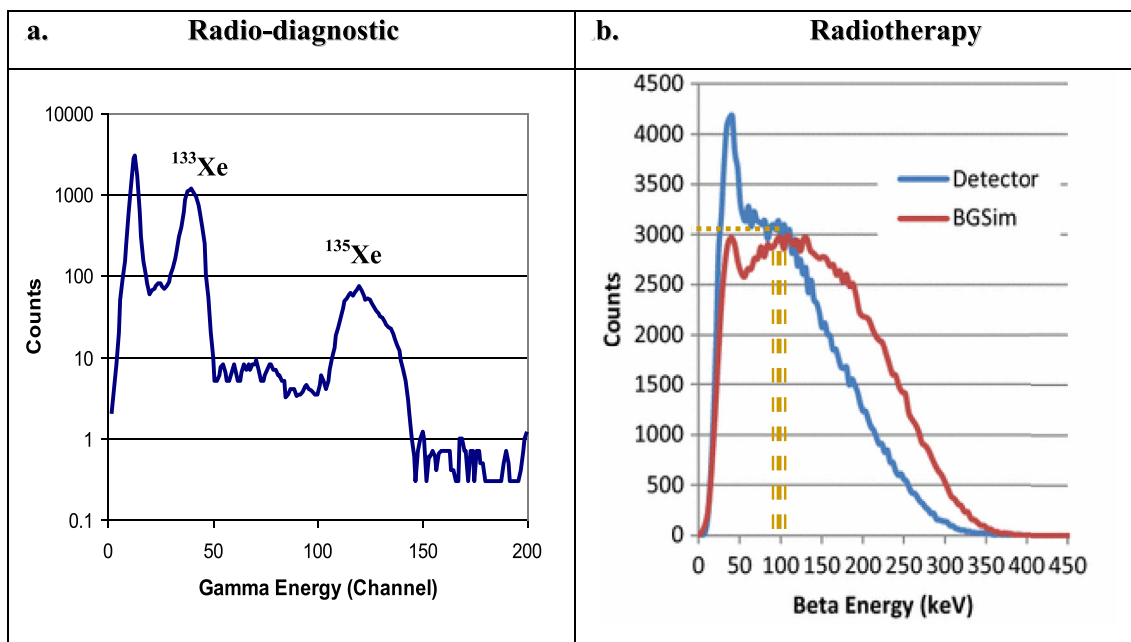


Fig. 3. Radioxenons γ data for in-situ assessment of their concentration as proposed by McIntyre et al. (2016), and β experimental and simulation (incorporated GEANT-modeled data sets from ^{133}Xe decay, as well as functionality to use nuclear detector-acquired data sets to create new beta spectra with varying amounts of background, ^{133}Xe , and its decay products).

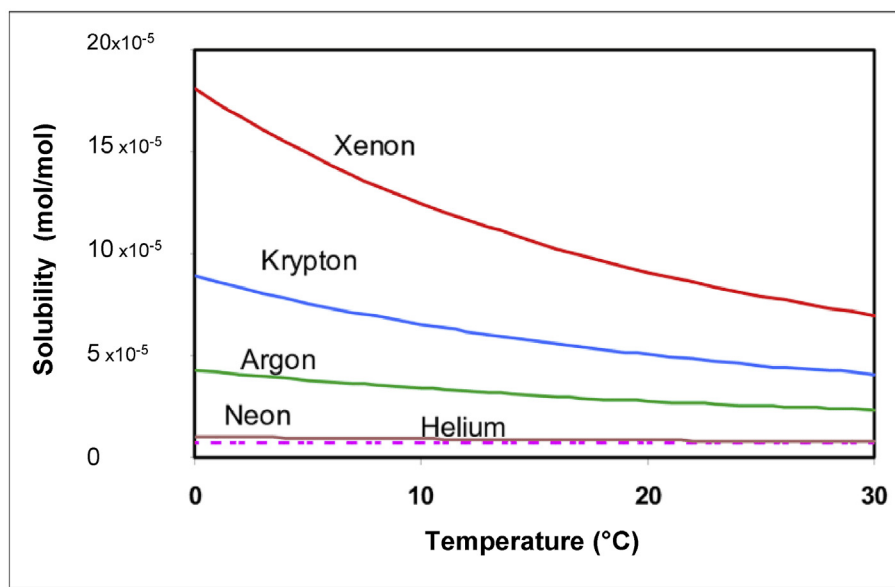


Fig. 4. Solubility of the noble gases in water (in mole of gas/mole of water) as a function of temperature (under 1 Atm) as reported by Moran et al. (2004) [51]. Note the solubility of Kr is about $\frac{1}{2}$ that of Xe in water.

tissues such as muscle or brain is between 60% and 300% of blood solubility. Measured solubility in biological tissues does not correspond well to solubility in water and oil. Most gases decrease in solubility by 1%–6% for each $^{\circ}\text{C}$ rise in temperature.

Inhaled [^{133}Xe]-xenon gas will enter the alveolar wall and enter the pulmonary venous circulation via the capillaries, however Xe also concentrates in fat nodules. Most of the [^{133}Xe]-xenon that enters the circulation from a single breath is returned to the lungs and exhaled after a single pass through the peripheral circulation (half-life 5.245 days). Xenon-133 is used for the diagnostic evaluation of pulmonary function and imaging, as well as assessment of cerebral blood flow. In the concentrations used for diagnostic purposes it is physiologically inactive.

However, the fat nodule may retain Xe significantly and virus (e.g. Corona) that has a lipid outer layer may concentrate Xe. It might be possible to attack such virus using beta radiation. The activity of the inhaled gas must be carefully quantified for diagnostics as well as for such a therapy. The later application must be carefully assessed. For ^{133}Xe the usual activity is 200–750 MBq, in children 10–12 MBq kg $^{-1}$. The minimum is 100–125 MBq.

The 3-phase ventilation scintigraphy with ^{133}Xe (single-breath, equilibrium and wash-out) should ensure a complete description of the physiological ventilation conditions and a sensitive test for obstructive airway diseases. However, the procedure is time-consuming and is therefore reduced in practice to a single single-breath exposure from

anterior (abdominal) or posterior (dorsal) view. Because of the low-energy radiation of ^{133}Xe in particular, the results of this procedure are now considered somewhat inaccurate. However accurate and fast tomographic reconstruction may solve the problem of ribs shadowing for example.

The xenon-33 delivery system by inhalation (such as ventilators or spirometers), and the associated tube assemblies must be sealed to avoid releasing radioactivity into the environment (which must be protected by a ventilation system). Medical use of xenon-133 in radiation therapy of cancer was initiated by Van Deripe (2000) [52].

The application of ^{133}Xe and comparison with the options offered by $^{219,222}\text{Rn}$ and ^{125}I may now be discussed. Risks are due to: release of ^{125}I , ^{131}I from the complex for example and these nuclides could fix on the thyroid and potentially induce cancer. $^{219,222}\text{Rn}$ induce by decay α emitter daughters that could fix on bone marrow inducing leukaemia.

These considerations make the use of ^{133}Xe very attractive.

6. Conclusion

During operation, a molten salt reactor produces noble gas radioisotopes bubbling from the liquid fuel. These versatile nuclear reactors which can be designed as very small modular reactors could be mounted and operated as source for the production of short-life radioisotopes. They could be adapted in a modern hospital context to produce electricity, heat, hydrogen and specific short-lived isotopes e.g. ^{133}Xe , ^{85}Kr . These noble gas radioisotopes can be sampled and treated for radiopharmaceutical applications including as tools for diagnostics using γ radiation or for specific viral diseases radiotherapy using the emitted β -particles. Among them ^{133}Xe is currently used for lung diagnostics thanks to its 80 keV γ . Its use could be extended to lung viral radiotherapy by utilising its 100 keV β^- (E_{mean}). The use of ^{85}Kr as a diagnostic and potential therapeutic agent is also examined, however its higher energy, lower solubility and longer half-life make it less attractive for radiotherapy. In this frame an effective and efficient krypton - xenon separation is needed. Emphasis is placed to zeolites and metal organic frameworks, taking into account the effect of temperature. Following an accurate radio-diagnostic, attention is given on potential lung viral therapeutic treatment e.g. CoViD using ^{133}Xe because of its potential dual ability (imaging and therapeutic tool). Comparison with the options offered by ^{219}Rn , ^{222}Rn and ^{125}I labelled reagent is discussed. While it is unlikely that treatment of SARS-CoV-2, mediated by a radiotherapy with ^{133}Xe , can lead to elimination of all virions, radiotherapy could be used in combination with other treatments e.g. antiviral drugs, see Gordon et al. (2020) [53] and consequently improve outcomes.

Declaration of competing interest

The authors declare that they have no known competing financial interests or personal relationships that could have appeared to influence the work reported in this paper.

References

- Crestoni ME. Radiopharmaceuticals for diagnosis and therapy reference module in chemistry. Molecular Sciences and Chemical Engineering 2018. <https://doi.org/10.1016/B978-0-12-409547-2.14205-2>.
- Parker JA, Coleman RE, Grady E, Royal HD, Siegel BA, Stabin MG, Sostman HD, Hilson AJW. SNM practice guideline for lung scintigraphy 4.0. J Nucl Med Technol 2012;40:57–65. <https://doi.org/10.2967/jnmt.111.101386>.
- Lull Robert J, Tatum James L, Sugeran Harvey J, Hartshorne Michael F, Kaplan Kenneth A. Radionuclide evaluation of lung trauma. Semin Nucl Med 1983; 13:223–37. [https://doi.org/10.1016/S0001-2998\(83\)80017-8](https://doi.org/10.1016/S0001-2998(83)80017-8).
- Graban W. Zastosowanie promieniotwórczego ksenonu (^{133}Xe) do badania wpływu glukozy i insuliny na spoczynkowy przepływ w mięśniowy. I. Metoda klirensu tkankowego z zastosowaniem promieniotwórczego ksenonu (^{133}Xe) [Use of radioactive xenon (^{133}Xe) for the studies on the effect of glucose and insulin on the rest blood flow. I. Tissue clearance method with application of radioactive xenon (^{133}Xe)]. Pol Przegl Radiol Med Nucl 1969;33(5):691–7.
- Bailey Dale L, Roach Paul J. A brief history of lung ventilation and perfusion imaging over the 50-year tenure of the editors of seminars in nuclear medicine. Semin Nucl Med 2020;50:75–86. <https://doi.org/10.1053/j.semnuclmed.2019.07.004>.
- Weinberg AM. Can we fix nuclear energy? Ann Nucl Energy 1979;6(9–10):473–82. [https://doi.org/10.1016/0306-4549\(79\)90019-7](https://doi.org/10.1016/0306-4549(79)90019-7).
- Elsheikh BM. Safety assessment of molten salt reactors in comparison with light water reactors. Journal of Radiation Research and Applied Sciences 2013;6:63–70. <https://doi.org/10.1016/j.jrras.2013.10.008>.
- Huke A, Ruprecht G, Weißbach D, Gottlieb St, Hussein A, Czserki K. The Dual Fluid Reactor – a novel concept for a fast nuclear reactor of high efficiency. Ann Nucl Energy 2015;80:225–35. <https://doi.org/10.1016/j.anucene.2015.02.016>.
- Zou Ch, Yu C, Wu J, Cai X, Chen J. Transition to thorium fuel cycle in a small modular molten salt reactor based on a batch reprocessing mode. Ann Nucl Energy 2020;138:107163. <https://doi.org/10.1016/j.anucene.2019.107163>.
- Kang X, Zhu G, Yan R, Liu Y, Cai X. Evaluation of ^{99}Mo production in a small modular thorium based molten salt reactor. Prog Nucl Energy 2020;124:103337. <https://doi.org/10.1016/j.pnucene.2020.103337>.
- Degueldre CA, Dawson RJ, Najdanovic-Visak V. Nuclear fuel cycle, with liquid ore and fuel: toward renewable. Sustainable Energy & Fuels 2019;3:1693–700. <https://doi.org/10.1039/C8SE00610E>.
- Smirnov MV, Korzun IV, Olegnikova VA. Hydrolysis of molten alkali chlorides, bromides and iodides. Electrochim Acta 1988;33:781–8. Electrochim. Acta, 33, 781-788 (1988).
- Eades MJ, Chaleff ES, Venneri PF, Blue ThE. The influence of Xe-135m on steady-state xenon worth in thermal molten salt reactors. Prog Nucl Energy 2016;93: 397–405.
- Wu J, Guo C, Cai X, Yu C, Chen J. Flow effect on ^{135}I and ^{135}Xe evolution behavior in a molten salt reactor. Nucl Eng Des 2017;314:318–25.
- Kallilainen J, Nischenko S. J. Krepel Evaporation of materials from the molten salt reactor fuel under elevated temperatures. J Nucl Mater 2020;533:152134.
- Akerib DS, Araújo HM, Bai X, Bailey AJ, Zhang C. Chromatographic separation of radioactive noble gases from xenon. Astropart Phys 2018;97:80–7.
- LeBlanc D. Driving change with IMSR. Nucl Eng Int 2018. 5 December.
- Pfenning G, Klewe-Nebenius H, Seelmann-Eggebert W. Chart of the nuclides forschungszentrum karlsruhe. 1998.
- Holden Norman E. 11. Table of the isotopes. In: Lide David R, editor. CRC handbook of chemistry and physics. 85th ed. Boca Raton, Florida: CRC Press; 2004.
- Incerti S, Kyriakou I, Bernal MA, Bordage MC, Francis Z, Guatelli S, Ivanchenko V, Karamitros M, Lampe N, Lee SB, Meylan S, Min CH, Shin WG, Nieminen P, Sakata D, Tang N, Villagrasa C, Tran HN, Brown JMC. Geant4-DNA example applications for track structure simulations in liquid water: a report from the Geant4-DNA Project. Med Phys 2018;45. <https://doi.org/10.1002/mp.13048>.
- Banerjee D, Simon CM, Elsaidi SK, Haraczyk M, Thallapally PK. Xenon gas separation and storage using metal-organic frameworks. Inside Chem 2018;4: 466–94. <https://doi.org/10.1016/j.chempr.2017.12.025>.
- Thallapally PK, Grate JW, Motkuri RK. Facile xenon capture and release at room temperature using a metal-organic framework: a comparison with activated charcoal. Chem Commun 2012;48:347–9. <https://doi.org/10.1039/c1cc14685h>.
- Jameson CJ, Jameson AK, Lim HM. Competitive adsorption of xenon and krypton in zeolite NaA: ^{129}Xe nuclear magnetic resonance studies and grand canonical Monte Carlo simulations. J Chem Phys 1997;107:4364–72. <https://doi.org/10.1063/1.474778>.
- Chen L, Reiss PS, Chong SY, Holden D, Jelfs KE, Hasell T, Little MA, Kewley A, Briggs ME, Stephenson A, et al. Separation of rare gases and chiral molecules by selective binding in porous organic cages. Nat Mater 2014;13:954–60. <https://doi.org/10.1038/nmat4035>.
- Chung YG, Haldoupis E, Bucior BJ, Haraczyk M, Lee S, Zhang H, Vogiatzis KD, Milisavljevic M, Ling S, Camp JS, et al. Advances, updates, and analytics for the computation-ready, experimental metal-organic framework database: CoRE MOF 2019. J Chem Eng Data 2019;64:5985–98. <https://doi.org/10.1021/acs.jced.9b00835>.
- Sikora BJ, Wilmer CE, Greenfield ML, Snurr RQ. Thermodynamic analysis of Xe/Kr selectivity in over 137000 hypothetical metal-organic frameworks. Chem Sci 2012; 3:2217–23. <https://doi.org/10.1039/c2sc01097f>.
- Ryan P, Farha OK, Broadbelt LJ, Snurr RQ. Computational screening of metal-organic frameworks for xenon/krypton separation. AIChE J 2011;57:1759–66. <https://doi.org/10.1002/aic.12397>.
- Wilmer CE, Leaf M, Lee CY, Farha OK, Hauser BG, Hupp JT, Snurr RQ. Large-scale screening of hypothetical metal-organic frameworks. Nat Chem 2011;4:83–9. <https://doi.org/10.1038/nchem.1192>.
- Simon CM, Mercado R, Schnell SK, Smit B, Haraczyk M. What are the best materials to separate a xenon/krypton mixture? Chem Mater 2015;27:4459–75. <https://doi.org/10.1021/acs.chemmater.5b01475>.
- Liu J, Thallapally PK, Strachan D. Metal-organic frameworks for removal of Xe and Kr from nuclear fuel reprocessing plants. Langmuir 2012;28:11584–9. <https://doi.org/10.1021/la301870n>.
- Banerjee D, Simon CM, Plonka AM, Motkuri RK, Liu J, Chen X, Smit B, Parise JB, Haraczyk M, Thallapally PK. Metal-organic framework with optimally selective xenon adsorption and separation. Nat Commun 2016;7:1831. <https://doi.org/10.1038/ncomms11831>.
- Cruciani G. Zeolites upon heating: factors governing their thermal stability and structural changes. J Phys Chem Solid 2006;67:1973–94. <https://doi.org/10.1016/j.jpcs.2006.05.057>.
- Park KS, Ni Z, Cò AP, Choi JY, Huang R, Uribe-Romo FJ, Chae HK, O'keeffe M, Yaghi OM. Exceptional chemical and thermal stability of zeolitic imidazolate frameworks. Proc Natl Acad Sci USA 2006;103:10186–91. <https://doi.org/10.1073/pnas.0602439103>.

- [34] Fernandez CA, Liu J, Thallapally PK, Strachan DM. Switching Kr/Xe selectivity with temperature in a metal-organic framework. *J Am Chem Soc* 2012;134:9046–9. <https://doi.org/10.1021/ja302071t>.
- [35] Ben-Mansour R, Qasem NAA. An efficient temperature swing adsorption (TSA) process for separating CO₂ from CO₂/N₂ mixture using Mg-MOF-74. *Energy Convers Manag* 2018;156:10–24. <https://doi.org/10.1016/j.enconman.2017.11.010>.
- [36] Huang A, Dou W, Caro J. Steam-stable zeolitic imidazolate framework ZIF-90 membrane with hydrogen selectivity through covalent functionalization. *J Am Chem Soc* 2010;132:15562–4. <https://doi.org/10.1021/ja108774v>.
- [37] Hasanzadeh A, Azamat J, Pakdel S, Erfan-Niya H, Khataee A. Separation of noble gases using CHA-type zeolite membrane: insights from molecular dynamics simulation. *Chem Pap* 2020;74:3057–65. <https://doi.org/10.1007/s11696-020-01139-9>.
- [38] Schneemann A, Bon V, Schwedler I, Senkovska I, Kaskel S, Fischer RA. Flexible metal-organic frameworks. *Chem Soc Rev* 2014;43:6062–96. <https://doi.org/10.1039/c4cs00101j>.
- [39] Yang Q, Jobic H, Salles F, Kolokolov D, Guillerm V, Serre C, Maurin G. Probing the dynamics of CO₂ and CH₄ within the porous zirconium terephthalate UiO-66(Zr): a synergic combination of neutron scattering measurements and molecular simulations. *Chem Eur J* 2011;17:8882–9. <https://doi.org/10.1002/chem.201003596>.
- [40] Chen L, Mowat JPS, Fairen-Jimenez D, Morrison CA, Thompson SP, Wright PA, Düren T. Elucidating the breathing of the metal-organic framework MIL-53(Sc) with ab initio molecular dynamics simulations and in situ X-ray Powder Diffraction Experiments. *J Am Chem Soc* 2013;135:15763–73. <https://doi.org/10.1021/ja403453g>.
- [41] Chen L, Grajciar L, Nachtigall P, Düren T. Accurate prediction of methane adsorption in a metal-organic framework with unsaturated metal sites by direct implementation of an ab initio derived potential energy surface in GCMC simulation. *J Phys Chem C* 2011;115:23074–80. <https://doi.org/10.1021/jp2090878>.
- [42] Qasem NAA, Ben-Mansour R. Adsorption breakthrough and cycling stability of carbon dioxide separation from CO₂/N₂/H₂O mixture under ambient conditions using 13X and Mg-MOF-74. *Appl Energy* 2018;230:1093–107. <https://doi.org/10.1016/j.apenergy.2018.09.069>.
- [43] Daglar H, Keskin S. Computational screening of metal-organic frameworks for membrane-based CO₂/N₂/H₂O separations: best materials for flue gas separation. *J Phys Chem C* 2018;122:17347–57. <https://doi.org/10.1021/acs.jpcc.8b05416>.
- [44] Adatoz E, Keskin S. Application of MD simulations to predict membrane properties of MOFs. *J Nanomater* 2015;2015:1–9. <https://doi.org/10.1155/2015/136867>.
- [45] Vitillo JG, Ricciardi G. Effect of pore size, solvation, and defectivity on the perturbation of adsorbates in MOFs: the paradigmatic Mg₂(dobpdc) case study. *J Phys Chem C* 2017;121:22762–72. <https://doi.org/10.1021/acs.jpcc.7b06252>.
- [46] Konik PA, Berdonosova EA, Savvotin IM, Klyamkin SN. The influence of amide solvents on gas sorption properties of metal-organic frameworks MIL-101 and ZIF-8. *Microporous Mesoporous Mater* 2019;277:132–5. <https://doi.org/10.1016/j.micromeso.2018.10.026>.
- [48] McIntyre JI, Schrom BT, Cooper MW, Prinke AM, Suckow TJ, Ringbom A, Warren GA. A program to generate simulated radionuclide beta–gamma data for concentration verification and validation and training exercises. *J Radioanal Nucl Chem* 2016;307:2381–7.
- [49] Yeh S-Y, Peterson RE. Solubility of carbon dioxide, krypton, and xenon in lipids. *J Pharmaceut Sci* 1963;52:453–8.
- [50] Weathersby PK, Homer LD. Solubility of inert gases in biological fluids and tissues: a review. *Undersea Biomed Res* 1981;7:277–96.
- [51] Moran J, Hudson GB, Eaton GF, Leif R. A contamination vulnerability assessment for the santa clara and san mateo county groundwater basins. UCRL-TR-203258 LLNL; 2004. <https://doi.org/10.2172/15009810>.
- [52] Van Derpe DR. Medical use of xenon-133 in radiation therapy of cancer. PAT; 2000US6358194.
- [53] Gordon CJ, Tchesnokov EP, Feng JY, Porter DP, Götte M. The antiviral compound remdesivir potently inhibits RNA-dependent RNA polymerase from Middle East respiratory syndrome coronavirus. *J Biol Chem* 2020;295:4773–9.